Frequency-difference EIT (fdEIT) using weighted difference and equivalent homogeneous admittivity: validation by simulation and tank experiment

2009 Physiol. Meas. 30 1087

(http://iopscience.iop.org/0967-3334/30/10/009)

IOP PUBLISHING PHYSIOLOGICAL MEASUREMENT

Physiol. Meas. **30** (2009) 1087–1099 doi:10.1088/0967-3334/30/10/009

Frequency-difference EIT (fdEIT) using weighted difference and equivalent homogeneous admittivity: validation by simulation and tank experiment

Sung Chan Jun[1], Jihyeon Kuen[2], Jeehyun Lee[3], Eung Je Woo[2], David Holder[4] and Jin Keun Seo[3]

[1] Department of Information and Communications, Gwangju Institute of Science and Technology, Korea
[2] College of Electronics and Information, Kyung Hee University, Korea
[3] Department of Mathematics, Yonsei University, Korea
[4] Department of Medical Physics and Bioengineering, University College London, UK

E-mail: ejwoo@khu.ac.kr

Received 8 May 2009, accepted for publication 18 August 2009
Published 9 September 2009
Online at stacks.iop.org/PM/30/1087

Abstract

A new method for producing frequency-difference images in electrical impedance tomography (EIT) has been recently suggested. It employed the use of a weighted voltage difference between two frequencies. In this paper, we first explain why the weighted difference is advantageous for some applications of the frequency-difference EIT (fdEIT). Based on a relationship between injection currents at two frequencies and a weighted difference of two corresponding complex voltages, we establish an fdEIT image reconstruction algorithm. In order to apply the algorithm to a practical setting, we propose the concept of an equivalent homogeneous admittivity whose value can be estimated by measuring induced voltages at the third frequency. To test this new fdEIT algorithm, we performed numerical simulations and imaging experiments using two-dimensional phantoms with frequency-dependent admittivity distributions. From reconstructed real- and imaginary-part fdEIT images, we could validate its advantage in terms of visualizing anomalies with fewer amounts of artifacts. We propose the method for applications in tumor or stroke imaging where we are mainly interested in contrast information within an fdEIT image. We suggest investigating the forward and inverse problems of an imaging domain with a frequency-dependent admittivity distribution, which has not been addressed rigorously until now.

Keywords: weighted frequency difference, EIT, admittivity image

(Some figures in this article are in colour only in the electronic version)

1. Introduction

When we inject current into an electrically conducting object such as the human body through surface electrodes, the internal current pathway and voltage distribution are determined by its admittivity (complex conductivity) distribution, geometry and electrode configuration. In this paper, we denote the admittivity as $\gamma = \sigma + i\omega\varepsilon$ in S m^{-1} where $\sigma, \omega, \varepsilon$ and $\omega\varepsilon$ are the conductivity, angular frequency, permittivity and susceptivity, respectively. In electrical impedance tomography (EIT), we measure the boundary voltage data resulting from multiple injection currents in order to reconstruct images of the admittivity distribution inside an object (Barber and Brown 1984, Webster 1990, Metherall *et al* 1996, Cheney *et al* 1999, Saulnier *et al* 2001, Holder 2005).

Static imaging in EIT has suffered from the fundamental ill-posedness combined with technical difficulties caused by a limited amount of measurable information, unknown boundary geometry, uncertainty in electrode positions, systematic measurement artifacts and random noise. In time-difference EIT (tdEIT), measured data at two different times are subtracted to produce images of changes in the admittivity distribution with respect to time. Since the data subtraction can effectively cancel out common errors, tdEIT has shown its potential as a new functional imaging modality in several clinical application areas (Holder 2005).

Since tdEIT requires time-referenced data, it is not applicable to cases where a single image in time is required or such time-referenced data are not available. Examples include imaging of tumors (Soni *et al* 2004, Kulkarni *et al* 2008, Trokhanova *et al* 2008) and cerebral stroke (McEwan *et al* 2006, Romsauerova *et al* 2006 and 2007). Noting that admittivity spectra of numerous biological tissues show frequency-dependent changes (Geddes and Baker 1967, Gabriel *et al* 1996, Grimnes and Martinsen 2008, Oh *et al* 2008), frequency-difference EIT (fdEIT) has been proposed to produce images of changes in the admittivity distribution with respect to frequency. Lately, frequency-difference magnetic induction tomography (fdMIT) has also been suggested for the detection of cerebral stroke.

In early fdEIT methods, frequency-difference images were formed by back-projecting the logarithm of the ratio of two voltages at two frequencies (Griffiths and Ahmed 1987a, 1987b, Griffiths 1987, Griffiths and Zhang 1989, Fitzgerald *et al* 1999, Schlappa *et al* 2000). More recent studies adopted the sensitivity matrix with a voltage difference at two frequencies (Yerworth *et al* 2003, Romsauerova *et al* 2006 and 2007, Bujnowski and Wtorek 2007). In MIT, induced voltage is proportional to the square of the frequency. For this reason, one should scale the voltage at the second frequency by the square of the ratio of two frequencies before any subtraction. Brunner *et al* (2006) and Zolgharni *et al* (2009a, 2009b) adopted this frequency scaling in their fdMIT methods. All of these fdEIT and fdMIT methods are basically utilizing a simple voltage difference at two frequencies and a linearized image reconstruction algorithm. Alternatively, we may consider separately producing two static (absolute) images at two frequencies and then subtract one from the other as suggested by Zolgharni *et al* (2009a) for fdMIT. This approach, however, will not be able to alleviate the technical difficulties of the static imaging method.

Recently, Seo *et al* (2008) suggested a new fdEIT method using a weighted voltage difference at two frequencies. They proposed two different contrast mechanisms in a reconstructed frequency-difference image. The first is the contrast in admittivity values between an anomaly and background. The second is the frequency dependence of an admittivity distribution to be imaged. Even though they demonstrated the feasibility of the new fdEIT method, there still remained several questions to be answered. First, we should understand why the use of a weighted voltage difference is advantageous in fdEIT. Second,

we must elaborate the fdEIT image reconstruction algorithm for more realistic cases where background admittivity distributions are inhomogeneous and change with frequency. Third, the algorithm must be validated by realistic numerical simulations and phantom imaging experiments. This paper addresses these three issues.

Since the admittivity spectra of most biological tissues changes with frequency, we will assume an imaging object with a frequency-dependent background admittivity in the development of fdEIT theory and numerical simulations. For phantom experiments, this means that we should not use a saline background. We will explain that a simple voltage difference between two frequencies should produce bigger artifacts when the background admittivity changes with frequency. After describing the reason why the weighted difference method is desirable, we will formulate a new fdEIT image reconstruction algorithm using the concept of an equivalent homogeneous admittivity. For the validation of the new method, we will show results of numerical simulations and phantom experiments using a 16-channel multi-frequency EIT (mfEIT) system KHU Mark1 (Oh *et al* 2007a, 2007b, 2008).

2. Methods

2.1. Problem definition

Let Ω be a two- or three-dimensional domain occupying an imaging object with its boundary $\partial\Omega$. Using an L-channel mfEIT system, we attach surface electrodes $\mathcal{E}_j$ for $j = 1, \ldots, L$ on $\partial\Omega$ and inject a sinusoidal current $I \sin(\omega t)$ between a chosen adjacent pair of electrodes. We assume that the current source and sink are connected to electrodes $\mathcal{E}_j$ and $\mathcal{E}_{j-1}$, respectively. Using the complete electrode model (Cheng *et al* 1989, Somersalo *et al* 1992, Vauhkonen *et al* 1999), the resulting complex time-harmonic voltage, denoted as u_ω^j, satisfies

$$\begin{cases} \nabla \cdot (\gamma_\omega(\mathbf{r}) \nabla u_\omega^j(\mathbf{r})) = 0 & \text{in } \Omega \\ \left(u_\omega^j + z_k \gamma_\omega \dfrac{\partial u_\omega^j}{\partial \mathbf{n}} \right) \Big|_{\mathcal{E}_k} = V_\omega^{j,k} & \text{for } \quad k = 1, \ldots, L \\ \gamma_\omega \dfrac{\partial u_\omega^j}{\partial \mathbf{n}} = 0 & \text{on } \quad \partial\Omega \setminus \cup_{k=1}^L \mathcal{E}_k \\ \int_{\mathcal{E}_k} \gamma_\omega \dfrac{\partial u_\omega^j}{\partial \mathbf{n}} = 0 & \text{if } \quad k \in \{1, \ldots, L\} \setminus \{j-1, j\} \\ \int_{\mathcal{E}_j} \gamma_\omega \dfrac{\partial u_\omega^j}{\partial \mathbf{n}} ds = I = -\displaystyle\int_{\mathcal{E}_{j-1}} \gamma_\omega \frac{\partial u_\omega^j}{\partial \mathbf{n}} \, \mathrm{d}s \end{cases} \tag{1}$$

where $\mathbf{r} = (x, y, z)$ is the position vector, z_k is the contact impedance of the kth electrode $\mathcal{E}_k$, $\mathbf{n}$ is the outward unit normal vector on $\partial\Omega$, $V_\omega^{j,k}$ is the complex voltage on $\mathcal{E}_k$ and γ_ω is the admittivity which depends on $\mathbf{r}$ and ω. Setting a reference voltage having $\sum_{k=1}^L V_\omega^{j,k} = 0$, we can obtain a unique solution u_ω^j of (1).

We assume that we have measured the boundary voltage $f_\omega^j := \left(V_\omega^{j,1} - V_\omega^{j,L}, V_\omega^{j,2} - V_\omega^{j,1}, \ldots, V_\omega^{j,L} - V_\omega^{j,L-1} \right) \in \mathbb{C}^L$ where $\mathbb{C}$ is the set of the complex number. Using the L-channel EIT system, we may inject L number of currents through adjacent pairs of electrodes and measure the following voltage data set:

$$\mathbf{f}_\omega = \left(f_\omega^1, f_\omega^2, \ldots, f_\omega^L \right) \in \mathbb{C}^L \times \mathbb{C}^L \times \cdots \times \mathbb{C}^L = \mathbb{C}^{L \times L}.$$

The reciprocity principle of $f_\omega^k(j) = f_\omega^j(k)$ indicates that only half of the data are independent. Three voltage data of $f_\omega^k(k-1)$, $f_\omega^k(k)$ and $f_\omega^k(k+1)$ are measured on one or both of current-carrying electrodes. Since they are influenced by the unknown electrode contact impedance,

we discard them. For these two reasons, $\mathbf{f}_\omega$ contains $\frac{L(L-3)}{2}$ number of independent data, which become the maximum degree of freedom in the imaging problem. In fdEIT, we inject currents with two frequencies of ω_1 and ω_2 to obtain corresponding voltage data sets $\mathbf{f}_{\omega_1}$ and $\mathbf{f}_{\omega_2}$, respectively. The goal is to visualize changes of the admittivity distribution between ω_1 and ω_2 by using two voltage data sets $\mathbf{f}_{\omega_1}$ and $\mathbf{f}_{\omega_2}$.

In tumor imaging or stroke detection using EIT, we are primarily interested in visualizing an anomaly from a background. This implies that we should reconstruct a local admittivity contrast. For a given injection current, however, the boundary voltage $\mathbf{f}_\omega$ is significantly affected by the background admittivity, boundary geometry and electrodes positions, while the influence of a local admittivity contrast due to an anomaly is much smaller. Since we utilize two sets of boundary voltage data, $\mathbf{f}_{\omega_1}$ and $\mathbf{f}_{\omega_2}$ in fdEIT, we need to evaluate their capability to perceive the local admittivity contrast. As in tdEIT, the rationale is to eliminate numerous common errors by subtracting the background component of $\mathbf{f}_{\omega_1}$ from $\mathbf{f}_{\omega_2}$, while preserving the local admittivity contrast component.

2.2. *Simple difference* $(\mathbf{f}_{\omega_2} - \mathbf{f}_{\omega_1})$ *cannot cancel out common errors*

The simple voltage difference $\mathbf{f}_{\omega_2} - \mathbf{f}_{\omega_1}$ may work well for an imaging object whose background admittivity does not change with frequency. A typical example is a saline phantom. For realistic cases where background admittivity distributions change with frequency, it will produce artifacts in reconstructed fdEIT images, as shown in section 3. To understand this, let us consider a very simple case where the imaging object has a homogeneous admittivity distribution, that is, $\gamma_\omega = \sigma_\omega + \mathrm{i}\omega\varepsilon_\omega$ is independent of the position $\mathbf{r}$. In such a homogeneous object, induced voltages $\bar{u}^j_{\omega_1}$ and $\bar{u}^j_{\omega_2}$ satisfy the Laplace equation with the same boundary data, and therefore the two corresponding voltage data vectors $\bar{\mathbf{f}}_{\omega_1}$ and $\bar{\mathbf{f}}_{\omega_2}$ are parallel in such a way that

$$\bar{\mathbf{f}}_{\omega_2} = \frac{\gamma_{\omega_1}}{\gamma_{\omega_2}} \bar{\mathbf{f}}_{\omega_1}.$$

When there exists a small anomaly inside the imaging object, we may assume that the induced voltages are close to the voltages without any anomaly. In other words, the voltage difference $\mathbf{f}_{\omega_2} - \mathbf{f}_{\omega_1}$ in the presence of a small anomaly can be expressed as $\mathbf{f}_{\omega_2} - \mathbf{f}_{\omega_1} \approx \bar{\mathbf{f}}_{\omega_2} - \bar{\mathbf{f}}_{\omega_1} = \frac{\gamma_{\omega_1}}{\gamma_{\omega_2}} \bar{\mathbf{f}}_{\omega_1} - \bar{\mathbf{f}}_{\omega_1} = \beta \bar{\mathbf{f}}_{\omega_1}$ for a complex constant β. This means that the simple difference $\mathbf{f}_{\omega_2} - \mathbf{f}_{\omega_1}$ significantly depends on the boundary geometry and electrode positions except the special case where $\mathbf{f}_{\omega_2} - \mathbf{f}_{\omega_1} = 0$. This is the main reason why the use of the simple difference $\mathbf{f}_{\omega_2} - \mathbf{f}_{\omega_1}$ cannot deal with common modeling errors even for a homogeneous imaging object.

2.3. *Why should weighted difference* $(\mathbf{f}_{\omega_2} - \alpha \mathbf{f}_{\omega_1})$ *be used in fdEIT?*

An imaging object including a background and anomaly has an admittivity distribution γ_ω which changes with frequency. We define a weighted difference of the admittivity at two different frequencies ω_1 and ω_2 as

$$\delta\gamma^{\omega_2}_{\omega_1} = \alpha\gamma_{\omega_2} - \gamma_{\omega_1} \tag{2}$$

where α is a complex number. We assume the following two conditions:

(i) in the background region, especially near the boundary, $\delta\gamma^{\omega_2}_{\omega_1} \approx 0$;
(ii) in the anomaly, $\delta\gamma^{\omega_2}_{\omega_1}$ is significantly different from 0.

In order to extract the anomaly from the background, we investigate the relationship between $\mathbf{f}_{\omega_2}$ and $\mathbf{f}_{\omega_1}$. We should find a way to eliminate the background influence while maintaining the information of the admittivity contrast across the anomaly. We decompose $\mathbf{f}_{\omega_2}$ into a projection part onto $\mathbf{f}_{\omega_1}$ and the remaining part:

$$\mathbf{f}_{\omega_2} = \alpha \mathbf{f}_{\omega_1} + \mathbf{h}_{\omega_2}, \qquad \alpha = \frac{\langle \mathbf{f}_{\omega_2}, \mathbf{f}_{\omega_1} \rangle}{\langle \mathbf{f}_{\omega_1}, \mathbf{f}_{\omega_1} \rangle} \tag{3}$$

where $\langle \cdot, \cdot \rangle$ is the standard inner product of two vectors. Note that $\mathbf{h}_{\omega_2}$ is orthogonal to $\mathbf{f}_{\omega_1}$.

In the absence of the anomaly, we may set $\gamma_{\omega_2} = \frac{1}{\alpha}\gamma_{\omega_1}$ and this results in $\mathbf{f}_{\omega_2} = \alpha \mathbf{f}_{\omega_1}$. Therefore, the projection term $\alpha \mathbf{f}_{\omega_1}$ mostly contains the background information, while the orthogonal term $\mathbf{h}_{\omega_2}$ holds the anomaly information. To be precise, $\alpha \mathbf{f}_{\omega_1}$ provides the same information as $\mathbf{f}_{\omega_1}$ which includes influences of the background admittivity, boundary geometry and electrode positions. The orthogonal term $\mathbf{h}_{\omega_2} = \mathbf{f}_{\omega_2} - \alpha \mathbf{f}_{\omega_1}$ contains the core information about a nonlinear change due to the admittivity contrast across the anomaly. This explains why the weighted difference $\mathbf{f}_{\omega_2} - \alpha \mathbf{f}_{\omega_1}$ must be used in fdEIT.

2.4. Frequency-difference image reconstruction algorithm

Applying a linear approximation (Cheney *et al* 1990, Lionheart *et al* 2005), we get the following relation:

$$\int_\Omega \delta\gamma_{\omega_1}^{\omega_2}(\mathbf{r}) \nabla u_{\omega_1}^j(\mathbf{r}) \cdot \nabla u_{\omega_2}^k(\mathbf{r})\, d\mathbf{r} \approx I \left(f_{\omega_2}^j(k) - \alpha f_{\omega_1}^j(k) \right), \qquad j,k = 1, \ldots, L. \tag{4}$$

Given α, we can reconstruct an image of $\delta\gamma_{\omega_1}^{\omega_2}$ using the weighted difference $\mathbf{f}_{\omega_2} - \alpha \mathbf{f}_{\omega_1}$. Since α is not known in practice, we need to estimate it from $\mathbf{f}_{\omega_2}$ and $\mathbf{f}_{\omega_1}$ using (3).

We discretize the imaging object Ω as $\Omega = \cup_{i=1}^N \Omega_i$ where Ω_i is the ith pixel. The number N should be limited by $N \leqslant \frac{L \times (L-3)}{2}$. Let χ_{Ω_i} be the characteristic function of the ith element Ω_i, that is, $\chi_{\Omega_i} = 1$ in Ω_i and zero otherwise. Let $\xi_1, \ldots, \xi_N$ be complex numbers such that $\sum_{i=1}^N \xi_i \chi_{\Omega_i}$ approximates $\sum_{i=1}^N \xi_i \chi_{\Omega_i} \approx \frac{\delta\gamma_{\omega_1}^{\omega_2}}{I\gamma_{\omega_1}\gamma_{\omega_2}}$. By approximating $\nabla u_\omega^j \approx \frac{1}{\gamma_\omega} \nabla U^j$ where U^j is the solution of (1) with $\gamma_\omega = 1$, it follows from (4) that

$$\begin{aligned} \sum_{i=1}^N \left(\xi_i \int_{\Omega_i} \nabla U^j(\mathbf{r}) \cdot \nabla U^k(\mathbf{r})\, d\mathbf{r} \right) &\approx \int_\Omega \frac{\delta\gamma_{\omega_1}^{\omega_2}}{I\gamma_{\omega_1}\gamma_{\omega_2}} \nabla U^j(\mathbf{r}) \cdot \nabla U^k(\mathbf{r})\, d\mathbf{r} \\ &\approx \left(f_{\omega_2}^j(k) - \alpha f_{\omega_1}^j(k) \right), \qquad j,k = 1, \ldots, L. \end{aligned} \tag{5}$$

The reconstruction method using the approximation (4) is reduced to reconstruct $\sum_{i=1}^N \xi_i \chi_{\Omega_i}$ that minimizes the following:

$$\sum_{j,k=1}^N \left| \sum_{i=1}^N \left(\xi_i \int_{\Omega_i} \nabla U^j(\mathbf{r}) \cdot \nabla U^k(\mathbf{r})\, d\mathbf{r} - \left(f_{\omega_2}^j(k) - \alpha f_{\omega_1}^j(k) \right) \right) \right|^2 \tag{6}$$

where α is the complex number described in section 2.3. In order to find $\xi = (\xi_1, \ldots, \xi_N)$, we compute the sensitivity matrix $\mathbb{A}$ the mnth entry of which is

$$a_{mn} = \begin{cases} \int_{\Omega_n} \nabla U^j \cdot \nabla U^k\, d\mathbf{r} & \text{if } |j-k| > 1 \\ 0 & \text{if } |j-k| \leqslant 1 \end{cases} \qquad (m = L(j-1)+k).$$

We can compute $\xi = (\xi_1, \ldots, \xi_N)$ by solving the following linear system through a truncated singular value decomposition (tSVD):

$$\mathbb{A}\xi = \mathbf{f}_{\omega_2} - \alpha \mathbf{f}_{\omega_1}.$$

It remains to compute the fdEIT image $\delta\gamma_{\omega_1}^{\omega_2}$ from the knowledge of ξ. We need to estimate the equivalent homogeneous (constant) admittivity $\hat{\gamma}_\omega$ corresponding to γ_ω to use the following approximation:

$$\delta\gamma_{\omega_1}^{\omega_2} \approx I\hat{\gamma}_{\omega_1}\hat{\gamma}_{\omega_2}\sum_{i=1}^{N}\xi_i\chi_{\Omega_i}.$$

From the divergence theorem, we obtain the following relation:

$$\frac{\hat{\gamma}_\omega}{\hat{\gamma}_0} = \frac{\hat{\gamma}_\omega}{\hat{\gamma}_0}\frac{\int_\Omega \nabla u^{k,\omega}\cdot\nabla u^{j,0}}{\int_\Omega \nabla u^{k,\omega}\cdot\nabla u^{j,0}} \approx \frac{f^{j,0}(k)}{f^{k,\omega}(j)} \quad \text{for any} \quad j,k\in\{1,2,\ldots,L\}.$$

For our 16-channel mfEIT system (Oh *et al* 2007a, 2007b, 2008), we may choose

$$\frac{\hat{\gamma}_\omega}{\hat{\gamma}_0} = \frac{1}{32}\sum_{j=1}^{16}\left(\frac{f^{j,0}(j+3)}{f^{j+3,\omega}(j)} + \frac{f^{j,0}(j-3)}{f^{j-3,\omega}(j)}\right) \tag{7}$$

where we identify $L+j=j$ and $-j=L-j$ for $j=1,2,3$.

In summary, we reconstruct an fdEIT image $\delta\gamma_{\omega_1}^{\omega_2}$ by

$$\delta\gamma_{\omega_1}^{\omega_2} = I\hat{\gamma}_{\omega_1}\hat{\gamma}_{\omega_2}\mathbb{A}^-\left(\mathbf{f}_{\omega_2}-\alpha\mathbf{f}_{\omega_1}\right) = I\hat{\gamma}_{\omega_0}^2\frac{\hat{\gamma}_{\omega_1}}{\hat{\gamma}_{\omega_0}}\frac{\hat{\gamma}_{\omega_2}}{\hat{\gamma}_{\omega_0}}\mathbb{A}^-\left(\mathbf{f}_{\omega_2}-\alpha\mathbf{f}_{\omega_1}\right) \tag{8}$$

where $\mathbb{A}^-$ is the pseudo-inverse of $\mathbb{A}$ estimated by the tSVD. In (8), $\frac{\hat{\gamma}_{\omega_1}}{\hat{\gamma}_{\omega_0}}\frac{\hat{\gamma}_{\omega_2}}{\hat{\gamma}_{\omega_0}}$ can be estimated from (7) using another low-frequency measurement $\mathbf{f}_{\omega_0}$. If we choose ω_0 low enough, $\hat{\gamma}_{\omega_0}$ may have a negligibly small imaginary part. In such a case, we may set $\delta\gamma_{\omega_1}^{\omega_2}/\hat{\gamma}_{\omega_0}^2$ as a reconstructed fdEIT image, which is equivalent to the complex image $\delta\gamma_{\omega_1}^{\omega_2}$ divided by an unknown real constant. In practice, it would be desirable to set ω_0 smaller than 1 kHz, for example 100 Hz.

This scaling will be acceptable for applications where we are mainly looking for a contrast change within an fdEIT image. These may include detections of tumors and strokes. In order to quantitatively interpret absolute pixel values of an fdEIT image, we must estimate the value of $\hat{\gamma}_{\omega_0}$, which requires the knowledge of the object size, boundary shape and electrode positions. Alternatively, we may estimate values of $\hat{\gamma}_{\omega_1}$ and $\hat{\gamma}_{\omega_2}$ in (8) without using the third frequency ω_0. This will again need geometrical information about the imaging object and electrode positions.

2.5. Numerical simulation

We performed numerical simulations on a unit disk $\Omega=\{(x,y): x^2+y^2<1\}$ with 16 electrodes equally spaced around its circumference. The electrode contact impedance of the complete electrode model in (1) was set to be 3000 Ω m^2. Since we discarded all the voltage data measured on one or both of current-carrying electrodes, the choice of this value is irrelevant in our case. Inside the disk, we placed an anomaly occupying the region $D=\{(x,y):(x+0.45)^2+y^2<0.15^2\}$. Admittivity values of the background and anomaly were adopted from measured values as described in the next section.

In all simulations, we used two frequencies of $\omega_1/2\pi = 5$ kHz and $\omega_2/2\pi = 50$ kHz as imaging frequencies and the third frequency of $\omega_0/2\pi = 1$ kHz for the estimation of equivalent homogenous admittivity values discussed in section 2.4. We numerically solved the forward problem in (1) to generate simulated data $\mathbf{f}_{\omega_1}$, $\mathbf{f}_{\omega_2}$ and $\mathbf{f}_{\omega_0}$. We added randomly a generated white Gaussian noise to the simulated data. The amounts of noise were 0.25% (relative to root mean square of noise-free simulated data) and 0.5% for the real and imaginary

Table 1. Measured admittivity values of six different materials including 0.5% saline, cylindrical pieces of cucumber, banana and carrot, mixture of carrot pieces with 1% saline and macerated banana at three different frequencies of 1, 5 and 50 kHz.

	Measured admittivity value in Sm^{-1}											
	0.5% saline		Cucumber		Carrot		Banana		Carrot+1% sal.		Mac. banana	
	σ	$\omega\varepsilon$	σ	$\omega\varepsilon$	σ	$\omega\varepsilon$	σ	$\omega\varepsilon$	σ	$\omega\varepsilon$	σ	$\omega\varepsilon$
1 kHz	0.130	0	0.044	0.004	0.023	0.011	0.035	0.016	0.208	0.102	0.221	0.109
5 kHz	0.130	0	0.051	0.015	0.031	0.012	0.043	0.017	0.208	0.103	0.228	0.110
50 kHz	0.130	0	0.105	0.076	0.100	0.050	0.102	0.052	0.232	0.123	0.283	0.150

part, respectively. The frequency-difference image $\delta\gamma_{\omega_1}^{\omega_2}$ was reconstructed based on (8). To examine the effects of the weighting complex number α, we tried the fdEIT algorithm twice by using the simple difference $\mathbf{f}_{\omega_2} - \alpha\mathbf{f}_{\omega_1}$ with $\alpha = 1$ and the weighted difference $\mathbf{f}_{\omega_2} - \alpha\mathbf{f}_{\omega_1}$ with $\alpha \neq 1$.

2.6. Phantom experiment

We constructed a two-dimensional phantom with 200 mm diameter, 100 mm height and 16 equally spaced stainless steel electrodes around its circumference. We filled the phantom with a chosen background material of 0.5% saline, mixture of carrot pieces with 1% saline or macerated banana (Romsauerova *et al* 2007). As an anomaly, we used a cylindrical piece of cucumber (4 mm diameter and 5 mm length), banana (3.6 mm diameter and 7.5 mm length) or carrot (4 mm diameter and 5.2 mm length).

We measured admittivity values of these six different materials using the four-electrode bioimpedance spectroscopy (BIS) method as described in Oh *et al* (2008). The time intervals between BIS measurements and imaging experiments were less than 10 min. We conducted both BIS measurements and imaging experiments at room temperature of about 25 °C.

Using the 16-channel mfEIT system KHU Mark1 (Oh *et al* 2007a, 2007b, 2008), we injected sinusoidal currents and measured boundary complex voltages between adjacent pairs of electrodes. The lowest reference frequency $\omega_0/2\pi$ introduced in section 2.4 was set to be 1 kHz. The imaging frequencies $\omega_1/2\pi$ and $\omega_2/2\pi$ were 5 and 50 kHz, respectively. We repeated the same experiment several times to check the reproducibility.

3. Results

3.1. Numerical simulation results

Table 1 summarizes measured admittivity values of six materials at three different frequencies of 1, 5 and 50 kHz. The lowest frequency of 1 kHz was used as the reference frequency $\omega_0/2\pi$ to evaluate the equivalent homogeneous admittivity in (7). The admittivity of 0.5% saline is resistive and show no frequency dependence in the range below 50 kHz. Other materials have both resistive and reactive components and their admittivity values change with frequency.

For the simplest case of a simulated cucumber against saline, both the simple and weighted difference approaches produced reasonably accurate images (figure 1). For the case of a homogeneous background admittivity (simulated macerated banana), both methods produced reconstructed images with spatial noise (figure 2). We estimated the noise level by computing the standard deviation of pixel values. The simple difference method produced noise that is

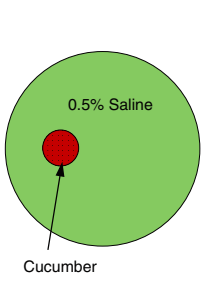

Frequency	Admittivity [S/m]	
	Saline	Cucumber
1 kHz	0.13	0.044+0.004i
5 kHz	0.13	0.051+0.015i
50 kHz	0.13	0.105+0.076i

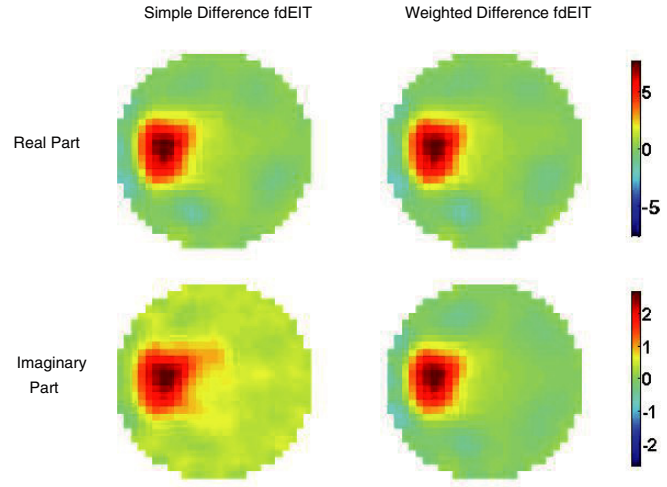

Figure 1. Numerical simulations of fdEIT image reconstructions using an imaging object including an anomaly of cucumber in a saline background. The simple difference method produced similar fdEIT images to those by using the weighted difference method since the background admittivity did not change much with frequency.

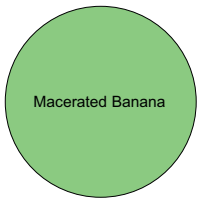

Frequency	Admittivity [S/m]
	Macerated Banana
1 kHz	0.221+0.109i
5 kHz	0.228+0.110i
50 kHz	0.283+0.150i

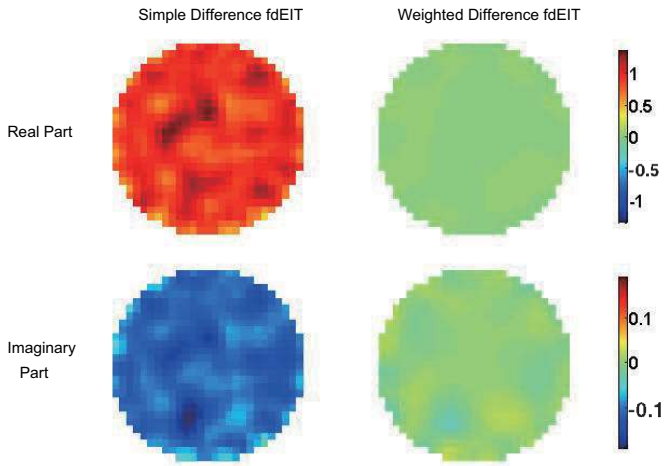

Figure 2. Numerical simulations of fdEIT image reconstructions using a homogeneous imaging object whose admittivity value changed with frequency. Reconstructed fdEIT images using the simple difference show severe artifacts even for the case of such a homogeneous model. Note that images using the weighted difference are free from artifacts.

4–25 times larger than that of the weighted difference method. For the case of the banana anomaly with the background of carrot pieces, the contrast between the anomaly and the background was ten times higher in the images produced by the weighted difference method (figure 3). Using the simple difference method, we may fail to extract the contrast information properly as explained in sections 2.2 and 2.3.

In figures 1 and 3, we scaled reconstructed fdEIT images using the weighted difference to have their maximum absolute contrasts equal to those of the simple difference. For the

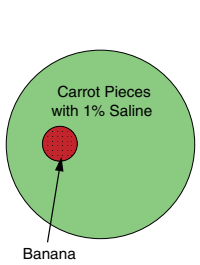

Frequency	Admittivity [S/m]	
	Carrot Pieces	Banana
1 kHz	0.208+0.102i	0.035+0.016i
5 kHz	0.208+0.103i	0.043+0.017i
50 kHz	0.232+0.123i	0.102+0.052i

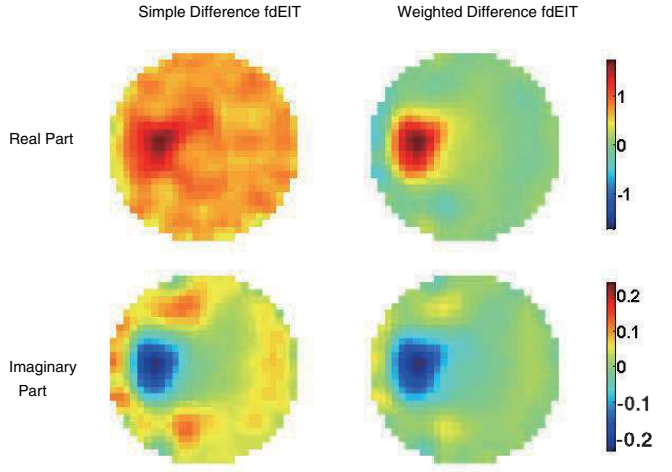

Figure 3. Numerical simulations of fdEIT image reconstructions using an imaging object including an anomaly of banana in a background of carrot pieces. Admittivity values of the anomaly and background changed with frequency. Reconstructed fdEIT images using the weighted difference distinguish the anomaly better than those by using the simple difference.

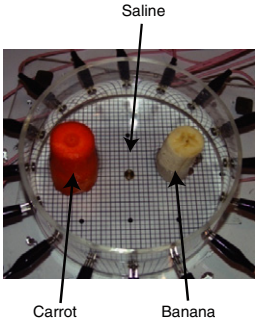

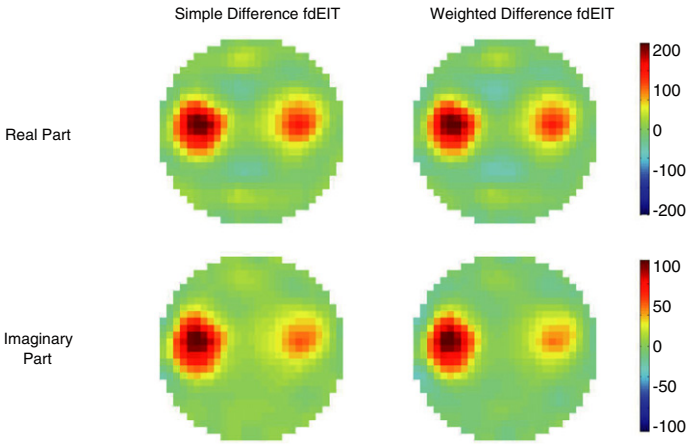

Figure 4. Imaging experiments using a phantom including two anomalies of carrot and banana in a saline background. Both of the simple and weighted difference method successfully produced fdEIT images since the background admittivity did not change much with frequency.

homogeneous case in figure 2, they were compared without scaling. For all numerical simulations, two fdEIT images to be compared were plotted within the same contrast value range.

3.2. Phantom experiment results

Both of the simple and weighted difference methods produced similar images of a saline phantom with two anomalies since the background admittivity did not change much with frequency (figure 4). We have tried two homogeneous phantoms whose conductivity values

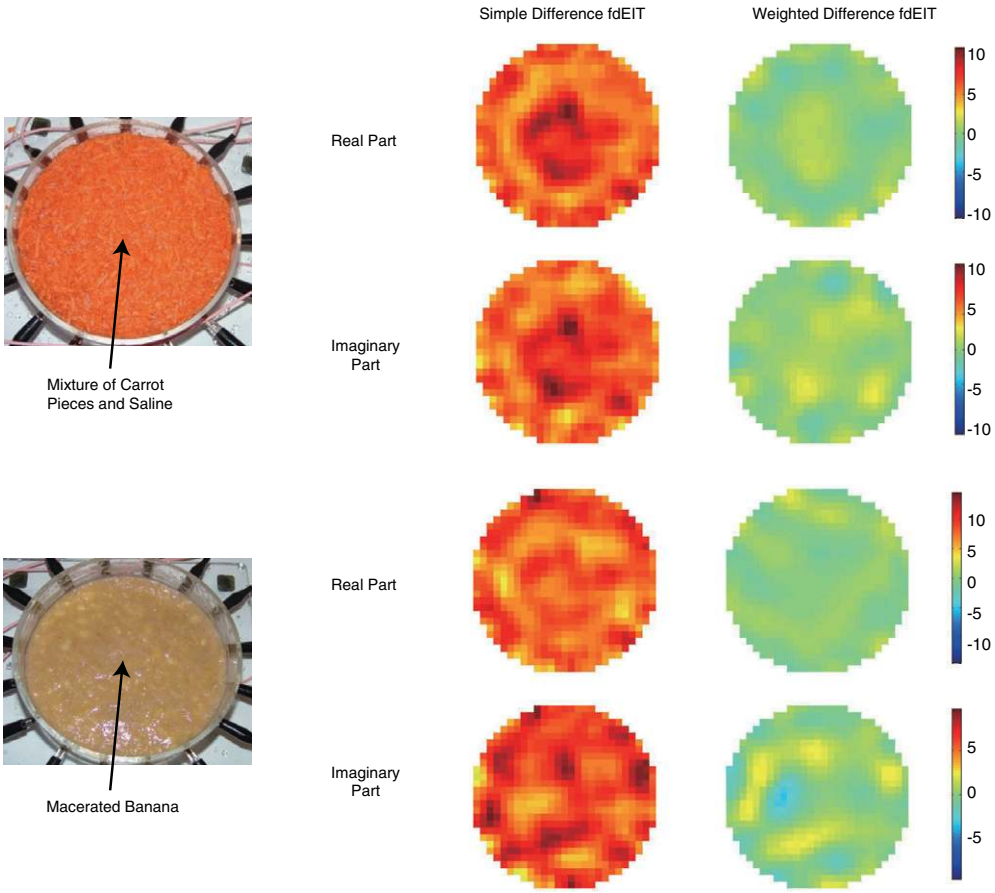

Figure 5. Imaging experiments using two homogeneous phantoms. One was filled with a mixture of carrot pieces and 1% saline. The other included macerated banana. Their admittivity values changed with frequency and the simple difference method produced fdEIT images with larger artifacts compared with those using the weighted difference method.

changed with frequency. One was filled with the mixture of carrot pieces and 1% saline and the other was filled with macerated banana. The simple difference method produced images with bigger artifacts compared with the weighted difference method (figure 5). The noise level was estimated to about three times larger in the images produced by the simple difference method. Placing a banana anomaly in one case and a carrot anomaly in the other case, we reconstructed fdEIT images of the two phantoms including the anomaly. The amounts of artifacts are larger in the images using the simple difference method, and the contrast of the anomaly with respect to the background was larger in the images produced by using the weighted difference method (figure 6).

4. Discussion and conclusion

For some applications of EIT including stroke detection and tumor imaging, fdEIT could be a promising alternative to static EIT imaging. In those cases, it is important to visualize a relative contrast between an anomaly and the background. When their admittivity values

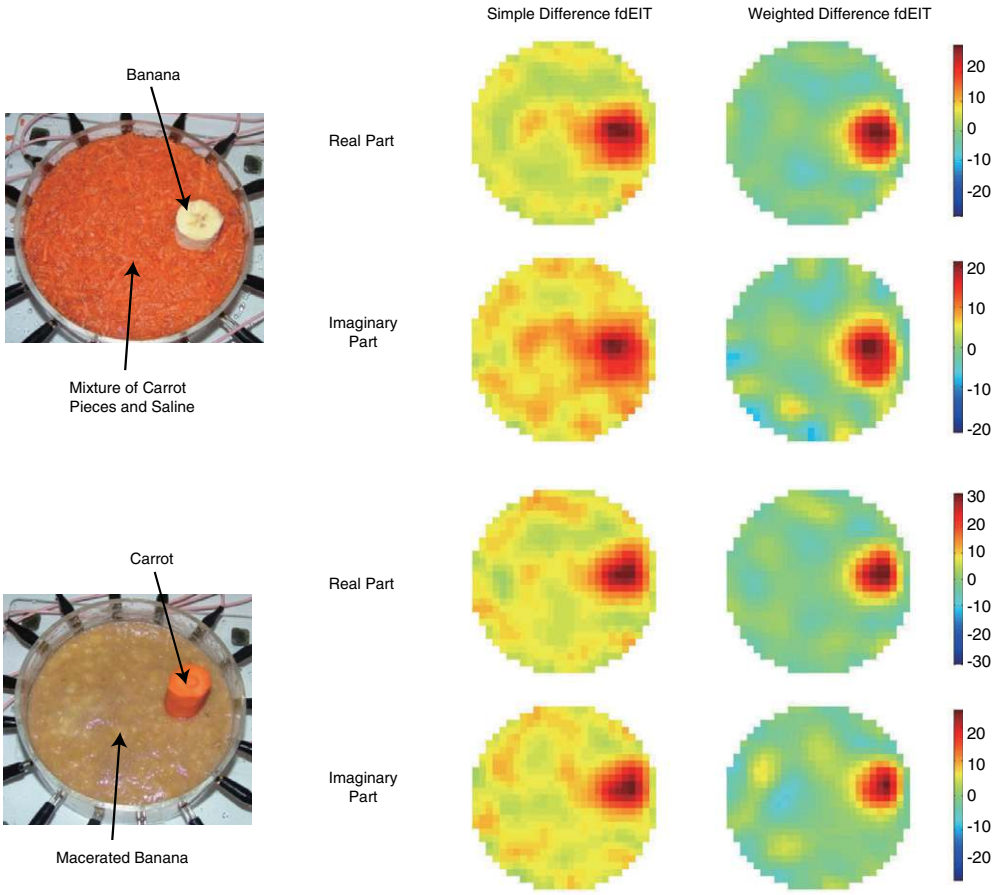

Figure 6. A banana or carrot anomaly was added to the first and second phantom in figure 5, respectively. Admittivity distributions of both phantoms changed with frequency, and the simple difference method produced fdEIT images with larger artifacts compared with those using the weighted difference method.

change with frequency, we found that the simple voltage difference between two frequencies fails to produce reliable fdEIT images.

The voltage difference is strongly influenced by the frequency dependence of the background admittivity distribution. In order to extract the effect of a local admittivity contrast due to the existence of an anomaly, we have proposed the use of a weighted frequency difference $\mathbf{f}_{\omega_2} - \alpha \mathbf{f}_{\omega_1}$ for fdEIT imaging. Both numerical simulations and phantom experiments show that the weighted difference method is superior to the simple difference method.

The proposed algorithm is based on the fact that the presence of an admittivity anomaly produces the component $\mathbf{h}_{\omega_2}$ of the data vector $\mathbf{f}_{\omega_2}$ at ω_2 in (3) that is orthogonal to the other data vector $\mathbf{f}_{\omega_1}$ at ω_1. This component $\mathbf{h}_{\omega_2}$ can be obtained from the weighted difference $\mathbf{f}_{\omega_2} - \alpha \mathbf{f}_{\omega_1}$. On the other hand, $\mathbf{f}_{\omega_2} - \alpha \mathbf{f}_{\omega_1} = 0$ for any homogeneous medium. The proposed weighted difference method is an effective way to extract a portion of useful data related with the anomaly while discarding unnecessary common background information.

Improvements in terms of the image reconstruction algorithm should be pursued including incorporation of a three-dimensional model and regularization. Compared with tdEIT, fdEIT requires an mfEIT system with much less systematic measurement errors (McEwan *et al* 2007). The current source must maintain its high output impedance and stability over the frequency range to be used in fdEIT imaging. All of the voltmeters implemented in a parallel system must have an identical frequency response that is close to the ideal one after calibration. We plan to upgrade the mfEIT system KHU Mark1 for better performance in fdEIT imaging.

In all application studies, we should note that the proposed fdEIT method using the weighted difference can provide only contrast information within an fdEIT image. Without knowing the geometrical data of the imaging object and electrode positions, absolute pixels values do not provide any quantitative information. Though the proposed fdEIT algorithm is promising for imaging the admittivity contrast of an anomaly such as blood in hemorrhagic stroke and cancer tissue in the breast, more thorough validation studies are needed including animal and human experiments. Since fdEIT is more robust against motion artifacts, we may also try a time series of fdEIT imaging for other applications including lung or stomach imaging.

Acknowledgments

This work was supported by the SRC/ERC program of MOST/KOSEF (R11-2002-103). Sung Chan Jun was supported by the National Research Foundation of Korea grant funded by the Korean Government (2009-0071225), GIST faculty start-up fund and the BioImaging Research Center at GIST. Jin Keun Seo and Jeehyun Lee were supported by the WCU program (R31-2008-000-10049-0).

References

Barber D C and Brown B H 1984 Applied potential tomography *J. Phys. E: Sci. Instrum.* **17** 723–33

Brunner P, Merwa R, Missner A, Rosell J, Hollaus K and Scharfetter H 2006 Reconstruction of the shape of conductivity spectra using differential multi-frequency magnetic induction tomography *Physiol. Meas.* **27** S237–48

Bujnowski A and Wtorek J 2007 An excitation in differential EIT—selection of measurement frequencies *IFMBE Proc. 13th Int. Conf. Elec. Bioimpedance and 8th Conf. EIT (Graz, Austria)* (Berlin: Springer) vol 13 pp 396–9

Cheney M, Isaacson D and Newell J C 1999 Electrical impedance tomography *SIAM Rev.* **41** 85–101

Cheney M, Isaacson D, Newell J C, Simske S and Goble J 1990 NOSER: an algorithm for solving the inverse conductivity problem *Int. J. Imag. Syst. Tech.* **2** 66–75

Cheng K S, Isaacson D, Newell J C and Gisser D G 1989 Electrode models for electric current computed tomography *IEEE Trans. Biomed. Eng.* **36** 918–24

Fitzgerald A, Holder A and Griffiths H 1999 Experimental assessment of phase magnitude imaging in multi-frequency EIT by simulation and saline tank studies *Ann. NY Acad. Sci.* **873** 381–7

Gabriel S, Lau R W and Gabriel C 1996 The dielectric properties of biological tissues: II. Measurements in the frequency range 10 Hz to 20 GHz *Phys. Med. Biol.* **41** 2251–69

Geddes L A and Baker L E 1967 The specific resistance of biological material: a compendium of data for the biomedical engineer and physiologist *Med. Biol. Eng.* **5** 271–93

Griffiths H 1987 The importance of phase measurement in electrical impedance tomography *Phys. Med. Biol.* **32** 1435–44

Griffiths H and Ahmed A 1987a A dual-frequency applied potential tomography technique: computer simulations *Clin. Phys. Physiol. Meas.* **8** 103–7

Griffiths H and Ahmed A 1987b Applied potential tomography for non-invasive temperature mapping in hyperthermia *Clin. Phys. Physiol. Meas. Suppl. A* **8** 147–53

Griffiths H and Zhang Z 1989 A dual-frequency electrical impedance tomography system *Phys. Med. Biol.* **34** 1465–76

Grimnes S and Martinsen O G 2008 *Bioimpedance and Bioelectricity Basics* (Oxford: Academic)

Holder D 2005 *Electrical Impedance Tomography: Methods, History and Applications* (Bristol: Institute of Physics Publishing)

Kulkarni R, Boverman G, Isaacson D, Saulnier G J, Kao T and Newell J C 2008 An analytical layered forward model for breasts in electrical impedance tomography *Physiol. Meas.* **29** S27–40

Lionheart W, Polydorides N and Borsic A 2005 The reconstruction problem *Electrical Impedance Tomography: Methods, History and Applications* ed D S Holder (Bristol: Institute of Physics Publishing)

McEwan A, Cusick G and Holder D S 2007 A review of errors in multi-frequency EIT instrumentation *Physiol. Meas.* **28** S197–215

McEwan A, Romsauerova A, Yerworth R, Horesh L, Bayford R and Holder D 2006 Design and calibration of a compact multi-frequency EIT system for acute stroke imaging *Physiol. Meas.* **27** S199–210

Metherall P, Barber D C, Smallwood R H and Brown B H 1996 Three-dimensional electrical impedance tomography *Nature* **380** 509–12

Oh T I, Koo W, Lee K H, Kim S M, Lee J, Kim S W, Seo J K and Woo E J 2008 Validation of a multi-frequency electrical impedance tomography (mfEIT) system KHU Mark1: impedance spectroscopy and time-difference imaging *Physiol. Meas.* **29** 295–307

Oh T I, Lee K H, Kim S M, Koo W, Woo E J and Holder D 2007b Calibration methods for a multi-channel multi-frequency EIT system *Physiol. Meas.* **28** 1175–88

Oh T I, Woo E J and Holder D 2007a Multi-frequency EIT system with radially symmetric architecture: KHU Mark1 *Physiol. Meas.* **28** S183–96

Romsauerova A, McEwan A, Fabrizi L and Holder D 2007 Evaluation of the performance of the multi-frequency electrical impedance tomography (MFEIT) intended for imaging acute stroke *IFMBE Proc. 13th Int. Conf. Elec. Bioimpedance and 8th Conf. on Electrical Impedance Tomography (Graz, Austria)* (Berlin: Springer) vol 13 pp 543–7

Romsauerova A, McEwan A, Horesh L, Yerworth R, Bayford R H and Holder D S 2006 Multi-frequency electrical impedance tomography (EIT) of the adult human head: initial findings in brain tumours, arteriovenous malformations and chronic stroke, development of an analysis method and calibration *Physiol. Meas.* **27** S147–61

Saulnier G J, Blue J C, Newell J C, Isaacson D and Edic P M 2001 Electrical impedance tomography *IEEE Sig. Proc. Mag.* **18** 31–43

Schlappa J, Annese E and Griffiths H 2000 Systematic errors in multi-frequency EIT *Physiol. Meas.* **21** 111–8

Seo J K, Lee J, Kim S W, Zribi H and Woo E J 2008 Frequency-difference electrical impedance tomography (fdEIT): algorithm development and feasibility study *Physiol. Meas.* **29** 929–44

Somersalo E, Cheney M and Isaacson D 1992 Existence and uniqueness for electrode models for electric current computed tomography *SIAM J. Appl. Math.* **52** 1023–40

Soni N K, Hartov A, Kogel C, Poplack S P and Paulsen K D 2004 Multi-frequency electrical impedance tomography of the breast: new clinical results *Physiol. Meas.* **25** 301–14

Trokhanova O V, Okhapkin M B and Korjenevsky A V 2008 Dual-frequency electrical impedance mammography for the diagnosis of non-malignant breast disease *Physiol. Meas.* **29** S331–44

Vauhkonen P J, Vauhkonen M, Savolainen T and Kaipio J P 1999 Three-dimensional electrical impedance tomography based on the complete electrode model *IEEE Trans. Biomed. Eng.* **46** 1150–60

Webster J G 1990 *Electrical Impedance Tomography* (Bristol: Adam Hilger)

Yerworth R J, Bayford R H, Brown B, Milnes P, Conway M and Holder D S 2003 Electrical impedance tomography spectroscopy (EITS) for human head imaging *Physiol. Meas.* **24** 477–89

Zolgharni M, Ledger P D and Griffiths H 2009a High-contrast frequency-difference imaging for magnetic induction tomography *Proc. 10th Conf. on Biomedical Applications of Electrical Impedance Tomography (Manchester, UK)*

Zolgharni M, Ledger P D and Griffiths H 2009b Imaging cerebral haemorrhage with MIT: frequency-difference imaging with a customized coil array *Proc. 10th Conf. on Biomedical Applications of Electrical Impedance Tomography (Manchester, UK)*